1384 *Biochemistry* **2011,** *50,* 1384–1395
DOI: 10.1021/bi1007518

BIOCHEMISTRY
including biophysical chemistry & molecular biology
Article

p38γ Activation Triggers Dynamical Changes in Allosteric Docking Sites[†]

Ramiro G. Rodriguez Limardo,[‡,§,⊥] Dardo N. Ferreiro,[‡,§,⊥] Adrián E. Roitberg,[∥] Marcelo A. Marti,[‡,§] and Adrian G. Turjanski*[,‡,§]

[‡]*Departamento de Química Inorgánica, Analítica y Química Física/INQUIMAE-CONICET, Facultad de Ciencias Exactas y Naturales, and* [§]*Departamento de Química Biológica, Facultad de Ciencias Exactas y Naturales, Universidad de Buenos Aires, Ciudad Universitaria, Pabellón 2, Buenos Aires C1428EHA, Argentina, and* [∥]*Department of Chemistry, University of Florida, Gainesville, Florida 32611-8435, United States.* [⊥]*Both authors contributed equally to this work*

Received May 12, 2010; Revised Manuscript Received December 28, 2010

ABSTRACT: Mitogen-activated protein kinases (MAPKs) are serine-threonine kinases that participate in signal transduction pathways. p38 MAPKs have four isoforms (p38α, p38β, p38γ, and p38δ) which are involved in multiple cellular functions such as proliferation, differentiation, survival, and migration. MAPK kinases phosphorylate p38s in the dual-phosphorylation motif, Thr-Gly-Tyr, located in their activation loop, which induces a conformational change that increases ATP binding affinity and catalytic activity. Several works have proposed that MAPK dynamics is a key factor in determining their function. However, we still do not understand the dynamical changes that lead to MAPK activation. In this work we have used molecular dynamics techniques to study the dynamical changes associated with p38γ activation, the only fully active MAPK crystallized so far. We performed MD simulations of p38γ in three different states, fully active with ATP, active without ATP, and inactive. We found that the dynamical fluctuations of the docking sites, important for protein−protein interactions, are regulated allosterically by changes in the active site. Interestingly, in the phosphorylated and ATP-bound states the whole protein dynamics lead to concerted motions of whole protein domains in contrast to the inactive state. The binding/unbinding of ATP participates in the reorientation of the two domains and in the regulation of protein plasticity. Our study shows that beyond the conformational changes associated with MAPK activation their correlated dynamics are highly regulated by phosphorylation and ATP binding. This means that MAPK plasticity may have a role in their catalytic activity, specificity, and protein−protein interactions and, therefore, in the outcome of the signaling network.

Mitogen-activated protein kinase (MAPK)[1] cascades are highly conserved signal transduction pathways coupling different extracellular signals to a variety of intracellular responses (*1*, *2*). The structural characteristics of MAPKs have been studied in great detail; members of ERK1/2, p38, and JNK groups have been all crystallized alone or in combination with substrates (*3*−*8*). These studies have provided a molecular understanding of the canonical MAPK domain structure (Figure 1 and Table 1). MAPKs are composed by two domains, an N-terminal domain formed largely by β-sheets and two helices, αC and αL16, and a C-terminal domain that is mostly helical, with four short β-strands that contain several residues involved in catalysis. The catalytic site, where the ATP and two magnesium ions bind, is at the junction between these two domains. A flexible linker between the N- and C-terminal domains allows their reorientation, and therefore it has been suggested that its conformation is important for the enzymatic activity (*9*). The MAPK insert, formed by two short helices located in the C-terminal domain, and a long loop that spans the whole protein, including the αL16 helix, distinguishes the MAPK's fold from the common one of the kinase superfamily. The family of p38 kinases includes four members known as p38α, p38β, p38γ (also known as SAPK3 or ERK6), and p38δ (*10*).The four isoforms share a Thr-Gly-Tyr phosphorylation motif in their activation loop and are stimulated by receptors and environmental stress conditions similar to those provoking the activation of JNKs (*11*). P38s MAPKs are involved in multiple cellular functions such as proliferation, differentiation, survival, and migration (*10*).

In order to achieve normal cellular functions, MAPK cascades should transduce signals with high efficiency and fidelity. However, the molecular basis for the mechanism underlying the specific reactions in the MAPK cascades has not been fully understood (*12*). MAPKs bind their upstream regulators (MAPKKs) and downstream targets by surface interactions that are achieved through docking motif binding sites that are outside of the catalytic domain. Emerging studies in the past few years have provided compelling evidence that these binding sites for docking motifs play a key role in determining the substrate

[†]The authors acknowledge the NSF Teragrid resource through Grant TG-MCA05S010 for providing computational resources and support that have contributed to the research results reported within this paper. This work was partially supported by grants from Universidad de Buenos Aires 08-X625 to M.A.M. and 08-X499 to A.G.T., ANPCYT 07-1650 to M.A.M. and 06-5203 to A.G.T., and Conicet PIP 01207 to M.A.M. and A.G.T.

*To whom correspondence should be addressed. E-mail: adrian@qi.fcen.uba.ar. Phone: 54-11-4576-3378 ext 220. Fax: 54-11-4576-3341.

[1]Abbreviations: ATP, adenosine triphosphate; MAPK, mitogen-activated protein kinase; DEJL, docking site for ERK and JNK, LXL; DEF, docking site for ERK, FXF; KSR, kinase suppressor of Ras; ERK, extracellular regulated kinase; JNK, c-Jun NH_2-terminal protein kinase; MAPKK, MAPK kinase; RMSD, root mean square deviation; RMSF, root mean square fluctuation; EM, essential mode.

 Published on Web 01/14/2011

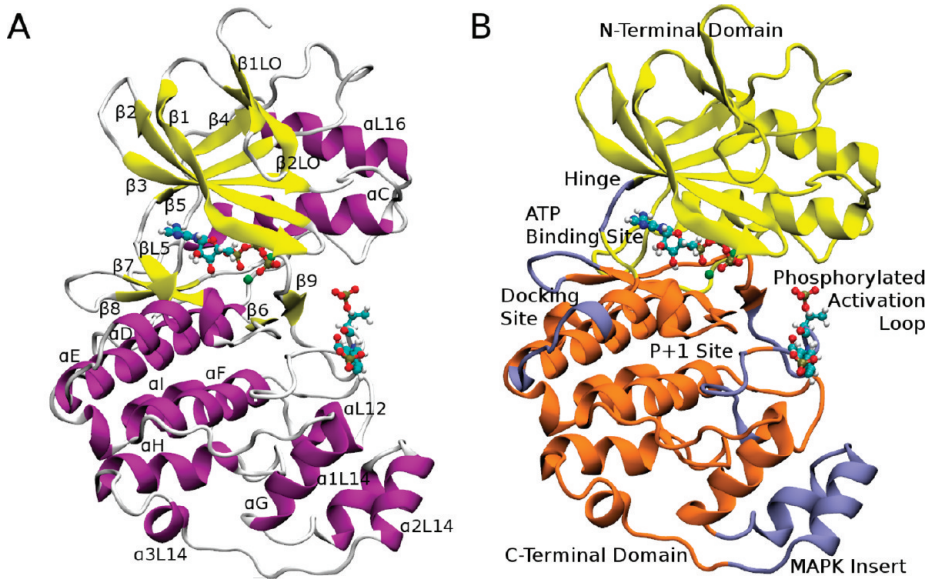

FIGURE 1: The structure of MAPKs. (A) Structure of activated p38γ (PDB: 1CM8) in cartoon representation. α-Helices are shown in purple, β-sheets in yellow, and loops in white. ATP and the phosphorylated residues are shown in ball and stick representation (red, oxygen; cyan, carbon; blue, nitrogen; white, hydrogen; gold, phosphorus; green, magnesium). (B) Cartoon representation: yellow, N-terminal domain; orange, C-terminal domain. In light blue we highlighted important motifs in the MAPK structure.

Table 1: Secondary Structure and Functional Regions of p38γ, As Defined by the Canonical MAPK Domain Structure

residue no.	secondary structure	functional region
12−16, 19−23	β1LO, β2LO	Nt-domain
27−36, 39−46, 52−58	β1, β2, β3	Nt-domain
66−81	αC	Nt-domain
91−93, 105−110	β4, β5	Nt-domain
111−113	loop	hinge region
114−115, 116−122	βL5, αD	Ct-domain
123−126	αD-αE loop	docking site
127−147	αE	Ct-domain
149−150, 159−162, 166−169, 176−177	β6, β7, β8, β9	Ct-domain
163−165	β7-β8 loop	docking site
178−186	loop	activation lip
183, 185		phosphorylation site
187−193		P + 1 site
194−199, 205−220, 231−242	αL12, αF, αG	(C-term)
247−252, 256−264	α1L14, α2L14	MAPK insert
273−276, 282−292, 302−311	α3L14, αH, αI	Ct-domain
337−348	αL16	Nt-domain

specificity of MAPKs (*13*). The best described docking motif is known as DEJL or D motif which possesses the general pattern $(Arg/Lys)_{1-2}$-$(X)_{2-6}$-$Ø_A$-X-$Ø_B$, where $Ø_A$ and $Ø_B$ are hydrophobic residues: leucine (*14*), isoleucine (Ile), or valine (Val) (*5*, *8*, *13*). Crystal structures of MAPK complexes with peptides derived from upstream and downstream targets having these DEJL motifs [e.g., ERK2 with MAPK phosphatase 3 (MK3) or with the hematopoietic tyrosine phosphatase (HePTP); p38α with the transcription factor MEF2 or the p38 MAPKK, MKK3B; and JNK1 with the scaffold Jun interacting protein-1 (JIP1)] have revealed that the MAPK binding site for the DEJL motif is similar among the different groups of MAPKs, comprising a hydrophobic groove between helices αD and αE and the β7-β8 reverse turn and an acidic patch that binds the positive amino acids within the DEJL motif of the partner protein (*5*, *15*, *16*). A second docking motif often found in MAPK substrates, such as the kinase suppressor of Ras (KSR) and the transcription factors Elk1 and SAP-1, has the amino acid sequence phenylalanine (Phe)-X-Phe-Pro and was termed DEF domain (docking site for ERK F*X*FP) (*13*, *17*, *18*). The DEF binding region in ERK2 was mapped to the P + 1 site, the αF helix, and the MAPK insert. Interestingly, a study conducting disruptive mutations of each of the ERK2 docking binding regions has shown that they can act independently and therefore may contribute to the regulation of distinct signaling events *in vivo*.

Recent studies have shown that dynamic conformational changes occurring on MAPKs upon phosphorylation, binding to ATP, upstream activators, scaffolds, and downstream targets may be important for MAPK activity and can regulate the assemblage of each MAPK module (*6*, *8*, *9*, *17*, *19*−*21*). It has been proposed that the binding of MAPKs to the docking motifs of their interacting partners may cause MAPKs to change their conformation and expose their activation loop, thereby becoming more accessible to MAPKKs and phosphatases (*6*, *8*, *9*, *17*, *19*−*21*). Dynamic changes have also been observed in the structure of ERK1/2 upon phosphorylation and ATP binding in sites located

far apart from the activation loop (*20*). However, most of the results that relate dynamics to function come from X-ray structures that despite having revealed new conformations give little information of the protein dynamics or hydrogen exchange and electron paramagnetic resonance experiments that give valuable information on protein dynamics but lack atomistic detail. Despite the great advance we have experienced in our understanding of how the MAPK module transmits the signal, we still do not have a clear picture of how these proteins work. Important questions remain open, such as: What is the effect of ATP binding on the protein dynamics? How does phosphorylation change MAPK dynamics? Are dynamical changes associated with protein activity? How do MAPKs regulate binding to scaffold proteins, upstream kinases, phosphatases, and targets that bind to the same docking site? How are complexes disassembled upon phosphorylation of the MAPKs or target proteins? Are MAPKs allosterically regulated? Taking this into account, we considered it worthwhile to conduct all atom molecular dynamics(*22*) simulations of a MAPK in different states as this technique allows us to follow with great detail the dynamical plasticity of the folded state in the nanosecond time scale.

MD simulations have been used extensively to understand how dynamics is coupled to function, and recent works have studied in detail the kinase fold (*23*, *24*).We conducted MD simulations of the MAPK p38γ since this protein is the only one fully crystallized in an active conformation with ATP and Mg^{2+}, making it a good model for our study. We used this complex as a starting conformation and constructed the phosphorylated protein without ATP and Mg^{2+} and the unphosphorylated protein. We performed long MD simulations of the different states and described in detail the structure of the previous uncharacterized structures of p38γ. We then analyzed the changes in the protein dynamics upon dephosphorylation and ATP unbinding. Our results show that dephosphorylation and ATP unbinding trigger allosteric transitions that significantly modify not only p38γ structure but dynamics, resulting in more coordinated motions in the activated/ATP bound protein. We found that the presence of ATP in the active state stabilizes the N-terminal domain and produces a change in the orientation between the two domains; however, the amplitude of the oscillations remains similar. Interestingly, by performing principal component analysis, we found that the MAPK insert is involved in the low-frequency essential modes and is among the most flexible moieties in the protein, suggesting that its conformation could be easily regulated by inter- or intraprotein interactions. The analysis of the simulations also revealed that dynamical fluctuations of the DEJL docking site are regulated by changes in the active site. Taking these observations into account, we propose that the observed changes in the dynamics of the docking sites, between the phosphorylated and unphosphorylated states and the ATP bound and unbound states, may be a way of regulating protein−protein binding affinities and therefore modulate the assembly/disassembly of the MAPK module. We finally discuss the population shift and stereochemical models of allostery in the context of p38γ activation mechanism. All together, we show that by performing MD simulations we are able to describe the structure and dynamics of p38γ with results that are in agreement with experimental results observed in other members of the MAPK family providing a broader picture of MAPK structure/dynamics to function relationships.

COMPUTATIONAL METHODS

Setup of the System and Equilibration. Protein coordinates were retrieved from the Protein Data Bank. The corresponding PDB codes are 1R3C for p38α (crystal resolution: 2.4 Å) (*25*) and 1CM8 for p38γ (crystal resolution: 2.0 Å) (*3*). In the structure corresponding to p38γ three loops are missing; therefore, we built them using as a template the p38α structure. The loops correspond to V33−A40 where the missing GSGAYG segment was inserted, the loop L314−Q322 where the sequence HDTEDEP was inserted, and the S329−R335 segment where FDDVD was inserted. Starting from the resulting p38γ complete structure (p38γ/p38α X-ray) obtained, three systems were built: p38γU, which is p38γ where we removed the ATP and dephosphorylated residues T183 and Y185; p38γP, which is p38γ phosphorylated in T183 and Y185 with the ATP removed from the active site; p38γP-ATP, which is p38γ phosphorylated in T183 and Y185 and bound to two Mg ions and ATP. The positions of the phosphorylated amino acids, the Mg, and the ATP were retrieved from the original crystal structure of p38γ (*3*).

Once the three initial structures were obtained, the following thermalization and equilibration protocol was performed in explicit solvent for all of the systems: Hydrogens were added with the tleap module of the AMBER 9 program, and the amber99-SB force field was used for the simulations (*26*, *27*). Standard protonation states were assigned to tritable residues (D and Q are negatively charged, K and R positively charged). Histidine protonation was assigned favoring formation of hydrogen bonds in the crystal structure. The parameters for phosphotyrosine and phosphoserine were taken from Craft et al. (*28*) and the ATP parameters from Meagher et al. (*29*). Each protein was immersed in a truncated octahedral box of TIP3P water (*30*). After the solvation the systems consist in 346 amino acids, over 10000 water molecules, and two Mg ions and ATP for p38γP-ATP. Each system was optimized using a conjugate gradient algorithm for 2000 steps. This optimization was followed by 100 ps long constant volume MD thermalization where the temperature of the system was slowly raised to 300 K. The heating was followed by a 100 ps long constant temperature and constant pressure MD simulation to equilibrate the system's density. During these processes the protein CA atoms were restrained by a 10 kcal/mol harmonic potential for the thermalization and a 1 kcal/mol harmonic potential for the density equilibration. After these equilibrations the systems ran for 10 ns at constant temperature and pressure as a final stabilization (*31*, *32*).

MD Simulations. For each system 125 ns long constant temperature and pressure MD simulations were performed with no restraint for the CA atoms. Pressure and temperature were kept constant with the Berendsen barostat and thermostat (*33*). All simulations were performed with periodic boundary conditions (*34*).

Essential Dynamics Analysis. In order to get insight into the dynamical properties of each structure and their influence on the coordination transitions, several essential dynamics (ED) analysis were performed for all production MD runs(*35*) using the ptraj module of the AMBER 9 program. The ED for each run (or combination of runs) is determined by diagonalizing the coordinate covariance matrices (Cov_{ij}) of the atomic positions along the desired trajectory, obtaining the corresponding eigenvalues and eigenvectors (eq 1)

$$Cov_{ij} = (1/M)\sum_{k}^{M}[X_i(k) - \langle X_i \rangle][\{X_j(k) - \langle X_j \rangle\}] \qquad (1)$$

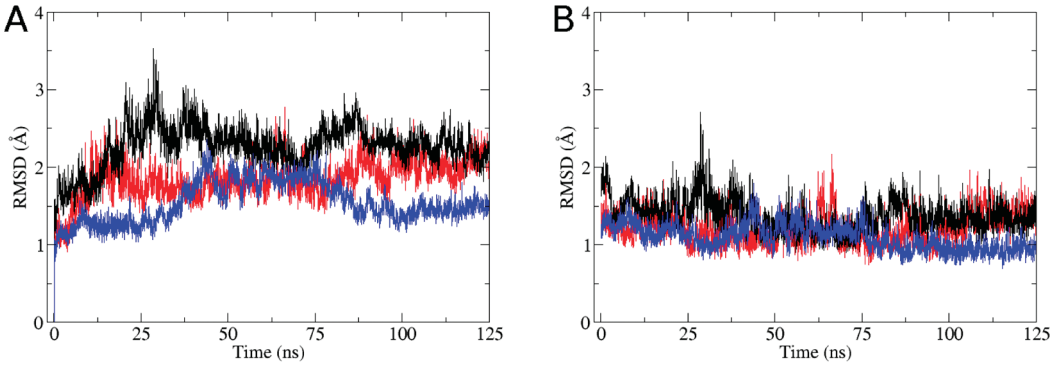

FIGURE 2: Cα RMSD vs time plot for the three 125 ns long MD simulations using as a reference either the initial complete structure (A) or the average structure (B) (as computed from the last 100 ns). Black line corresponds to p38γU, red line to p38γP, and blue line to p38γP-ATP.

where the sum goes over the "M" configurations or snapshots from the dynamics, $X_i(k)$ corresponds to ith Cartesian coordinate of the system in snapshot number k, and $\langle X_i \rangle$ represents the mean value of X_i along the MD simulation.

After diagonalization each obtained eigenvector (v_i) corresponds to an essential mode (EM) of the protein. Together, all of the EMs describe the motions of the protein along the MD run used to generate the computed matrix. The eigenvalues (λ_i) obtained represent the relative contribution of each EM to the overall motions, with the first EM being the one with major contribution or larger eigenvalue. The ED was computed only for the backbone (N, C, CA, O) atoms. The EM for each individual MD run was computed and analyzed. Then the EMs of combined trajectories were computed to gain deeper insight into the structural transition between both simulations. In this combined MD analysis the first EM (V_1) is able to extract the concerted movement corresponding to the transition between both states, used to compute the covariance matrix, and will be called a transition EM.

Projections "$P_N(t)$" along the MD runs onto selected EMs were also performed to analyze the configurational space explored along the MD run (eq 2)

$$P_N(t) = v_N \cdot r(t) \tag{2}$$

where v_N is the Nth EM and $r(t)$ is the protein conformation at time t. Projections are measured in angstroms, and the value corresponds to the overall deviation from the mean structure along the projected mode. After projecting the selected MD simulation along the selected mode, the normalized histograms were computed.

Based on the comparison of the equilibrium and transition EM, a slightly modified version of the involvement coefficients (IC) of each EM to the transition is computed (eq 3):

$$\mathrm{IC} = v_{\mathrm{A}j} \cdot V_{\mathrm{AB}} \tag{3}$$

In eq 3, $v_{\mathrm{A}j}$ is the j^{th} EM of equilibrium simulation of the A state, whereas V_{AB} corresponds to the transition EM computed by combining the A and B trajectories. In this case IC expresses how much of the structural transition between states A and B is contained in the EM number "j" of MD corresponding to the A state. This method, therefore, allows to analyze how much of the natural motions of the protein in a given state contribute to the selected conformational transition. This type of analysis based on the essential dynamics has already proven useful in the study of the structural and dynamical relationships in several proteins including the study of structural transitions (*36*, *37*).

Entropy Calculation. To analyze the change in entropy in the activation process of p38γ, we estimated the configurational entropy of the three different states by using the quasi-harmonic approximation (*38*). In the quasi-harmonic analysis the entropy is obtained by the construction of the $3N \times 3N$ covariance matrix of the MD followed by the numerical diagonalization to obtain the EM and their corresponding eigenvalues as described above. We computed the entropy by increasing the sampling windows by 1 ns intervals including always the same number of snapshots for each window.

RESULTS

The results are organized as follows: Initially the stability of the simulations is presented. Then, the structural changes between the states are presented, and the dynamics of each state is analyzed in detail followed by a comparison of the dynamics between the three states. Finally, we analyze the population shift and stereochemical models in the context of MAPK activity. The states are named p38γP-ATP for the complex of phosphorylated p38γ with ATP and Mg ions, p38γP for the phosphorylated protein, and p38γU for the unphosphorylated/inactive state.

Stability of the MD Simulations. Given the length of the presented MD simulations, our first analysis concerns the stability of each of the three studied systems: p38γU, p38γP, and p38γP-ATP. Figure 2 shows the RMSD vs time plot for the three simulations using as a reference either the initial complete structure (built as described in Computational Methods) or the average structure computed for the last 125 ns.

As can be seen in Figure 2A, the three systems display moderated RMSD values using the p38γP-ATP X-ray structure as a reference (*3*). As expected, p38γP-ATP (blue line) has the lowest RMSD, because this is the state corresponding to the original structure. RMSD plots show that there is an initial fast equilibration of less than 1 ns in all systems. After this, p38γU (black line) continues to drift from the initial structure for about 30−35 ns when a stable conformational ensemble is obtained; consistently for p38γP (red line) this drift lasts about 10−25 ns. Figure 2B clearly shows that after these initial equilibrations, all conformational ensembles remain stable with RMSD values of less than 2 Å with respect to the average structure.

We also evaluated the stability of the simulations by analyzing the essential modes computed as described in Computational Methods. Usually, for proteins, most structural variance is captured by only a few collective motions, which are described by the first essential modes (*39*). These EMs can thus be used to characterize the dominant dynamical behavior of a given protein.

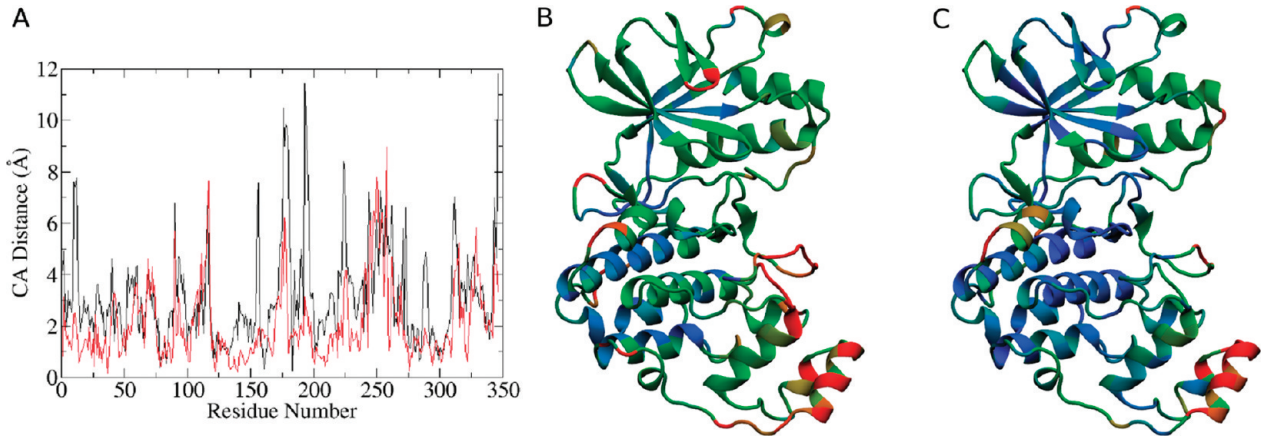

FIGURE 3: (A) Backbone comparison: black for p38γU vs p38γP; red for p38γP vs p38γP-ATP. Schematic representation of the observed differences for p38γU vs p38γP (B) and p38γP vs p38γP-ATP (C). Blue represents distances lower than 2 Å, green distances range between 2 and 4 Å, and red distances are higher than 4 Å.

Furthermore, projections of the trajectory along these EMs also show how the conformational space is sampled along the simulation. The corresponding results for each system are presented in the Supporting Information (Figures S1 and S2). The EM projection vs time plot shows that no significant drift seems to be present and that sufficient sampling along the conformational space is achieved pointing to a reasonable convergence of the simulations. However, we cannot rule out that, for the most flexible regions of the proteins, longer times are needed to fully achieve convergence. This may be the case for the MAPK insert, which is one of the most flexible regions of this protein. As discussed in detail below, the region encompassing the MAPK insert significantly contributes to the first essential modes, and its dynamics is greatly regulated by the protein state. For example, as shown in Supporting Information Figure S2B, a late drift in the projection of the first mode of p38γP is present which is associated to a rotation of helix α1L14 of the MAPK insert that is sampled at the end of the simulation.

To further analyze convergence of each state dynamics, we computed the conformational entropy, derived from the complete set of EMs, for increasing time intervals from 0 to 125 ns, with a sampling window of 1 ns. The corresponding figure, Supporting Information Figure S5, shows how the entropy slowly converges, strongly suggesting that conformational sampling convergence is achieved in the time scale of the simulation.

Is important to remark that although complete convergence is difficult to achieve, we present conclusive evidence that after an initial relaxation time new conformational states are reached corresponding to structures that, as we will discuss below, are in accord to the conformational changes observed for other MAPKs. Taking this into account, all of the data calculated in this paper, RMSF, average structures, essential modes, and geometrical measurements are computed only on the equilibrated last segment of the simulations where the structure has ceased to drift.

Structural Comparison of p38γ in the Different States. As the only crystallized structure of p38γ is p38γP-ATP, we first determined a representative structure of the dynamics of the three systems and then calculated the differences between them. In order to obtain a representative structure of the dynamics, we selected the one having the minimum cumulative RMSD to each snapshot in the simulation using the program kclust. The global RMSD difference is 2.4 Å between the representative structures of p38γU and p38γP and 1.7 Å between p38γP and p38γP-ATP. The structural changes between states are small, as has been previously observed for other MAPKs, which may indicate that changes in protein dynamics are the ones regulating protein function. Figure 3A shows the CA distance vs residue plot between the inactive and phosphorylated structure (black) and between the active and ATP-bound structure (red), while in Figure 3B,C the comparison is shown colored on the MAPK structure.

The changes upon dephosphorylation appear in several zones, as expected; the more pronounced effects are observed in the phosphorylation lip and in residues nearby. Unexpectedly, there are big changes in the whole MAPK insert and in the DEJL docking site. Moderate changes are also observed in the N-terminal domain loops β1-β2L0 and β4-β5. Finally, changes in the long loop between αI and αL16 are also observed.

The structural changes due to ATP binding to p38γP structure are smaller (compare black and red lines). Surprisingly, the phosphorylation lip is not significantly modified, but major changes are observed in the MAPK insert and in the loop αD-αE, part of the DEJL docking site. These results indicate that there are conformational changes in regions which are not directly interacting with the phosphorylated residues and that have been associated with protein−protein interactions.

The modeled structures, p38γU and p38γP, could be in principle compared with the abundant previously crystallized structures of other MAPKs. However, this is not an easy task given that most of the structures solved so far have drugs in the active site or peptides in the docking site or are mutant proteins. In this sense, there are two structures of p38α (1WFC and 1R3C (the latter is a one point mutation)) in the unphosphorylated state, one structure of p38β (3COI), one of ERK2 (1ERK), and one of ERK3 (2I6L). The p38γU representative structure is very similar to these structures despite the expected changes in the conformation of the MAPK insert, the activation loop, and the long loop between helices αI and αL16, which are distinctive of each family member. However, and consistent with our *in silico* model, inactive MAPK displays usually a partially solvent exposed activation loop. Considering the phosphorylated structure, removing ATP results in small structural changes, since the loop remains tightly bound due to phosphate−protein interactions. A rigid protein-bound loop structure for the phosphorylated ATP free state is consistent with the only other active structure of ERK2 (2ERK) due to the strong interactions of the

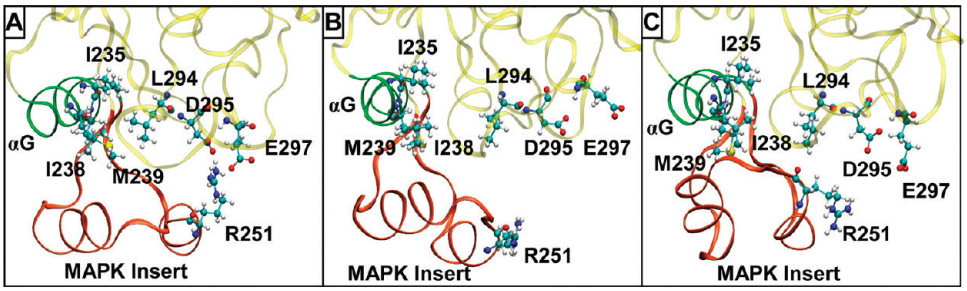

FIGURE 4: Changes in the MAPK insert upon activation and ATP binding: (A) p38γU; (B) p38γP; (C) p38γP-ATP. In all cases the protein backbone is represented as a tube, the MAPK insert is shown in orange color, helixG is in green; and the rest of the protein is in yellow. The amino acids that change their interaction in the different states are depicted as ball and stick (oxygen is in red, nitrogen is in blue, hydrogen is in white, sulfur is in yellow, and carbon is in cyan).

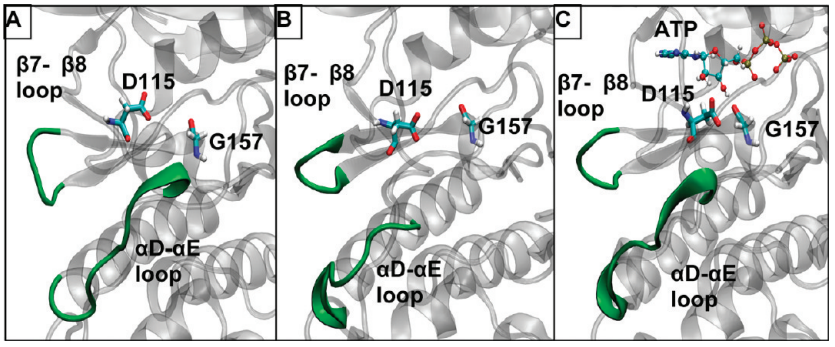

FIGURE 5: Changes in the DEJL docking site due to ATP binding: (A) p38γU; (B) p38γP; (C) p38γP-ATP. In all cases the protein backbone is represented as cartoon rendering, the two loops forming the DEJL docking site, αD-αE loop and β7-β8 loop, are in green, and the rest of the protein is in gray color. D115 and G157 are depicted as tubes, and ATP is depicted as ball and stick (oxygen is in red, nitrogen is in blue, hydrogen is in white, phosphate is in brown, and carbon is in cyan).

phosphate with conserved arginines. Despite the global changes there are interesting changes in the MAPK sites important for protein−protein interactions that are explained in detail below.

To further characterize the structural differences between the states, we calculated the contact map (*40*) for the average structures of each state (Supporting Information Figures S8 and S9). We then compared the contact maps and analyzed the regions that changed upon protein activation and ATP binding. We found that in the P38γU state the MAPK insert region establishes different contacts when compared to the other two states. The interaction of residues I235, I238, and M239 with L294 is lost in the P38γP and P38γP-ATP states, together with the interaction of R251 with D295 and E297 that only appear in the inactive state. In the MD simulations we observed that the salt bridges formed between R251 and the two acidic residues, D295 and E297, that are only formed in the P38γU state induce a conformational change in the whole MAPK insert moiety moving away helices α1L14 and α2L14 from helix G (Figure 4). In the phosphorylated and ATP-bound states αG is interacting with α1L14; however, upon movement of the MAPK insert the hydrophobic residues of helix G (I235, I238, and M239) are free to interact with L294. Furthermore, we can find the pathway of interactions that changed upon dephosphorylation if we look at the contact map and the molecular dynamics simulations. In the phosphorylated state, T204 has a hydrogen bond with R299 moving the loop, that shares with D295 and E297, toward the activation loop that keeps the acidic residues away from interacting with R251. As the arginine from the MAPK insert is unable to form the salt bridge with the two acidic residues, the MAPK insert remains near αG. However, in the inactive state, T204 is interacting with S180 by a hydrogen bond that impairs its interaction with R299. S180 changes its conformation due to the reorganization of the activation loop upon dephosphorylation. A change in the activation loop triggers a change in the MAPK insert and therefore allosterically regulates its conformation. Similarly, in ERK2, we see that a salt bridge is formed between the MAPK insert and the loop that connects helices αH and αI, only in the inactive state (PDB: 1ERK) (Supporting Information Figure S10), and there is a change in the position of the whole MAPK insert. However, the pathway of interactions could be different, as the activation loop in ERK is longer and the change upon dephosphorylation of the activation loop is more dramatic. The presence of basic and acidic amino acids located near in space and belonging to the MAPK insert and the αH-αI loop is also conserved in p38α and JNK1 proteins. Together, this evidence suggests that the presence or absence of a salt bridge between these two moieties could be important in p38γ and also in other MAPKs.

Another site important for protein−protein interactions is the DEJL docking site. If we analyze the contact map, we see a change in the interactions of residues 160−167 and 120−127 between the p38γP and p38γP-ATP states. The ATP molecule makes interactions with several amino acids in the MAPK active site; among them, D115 and G157 interact with the two hydroxyl groups of the ribose. These interactions are of paramount importance for the dynamics of the DEJL docking site; D115 is forming a short βL5 and is located just at the beginning of αD. G157 is at the end of the loop where β7 begins. In the ATP-bound state these two residues are near in space because they both interact with the ribose moiety (Figure 5C). Interestingly, in the ATP-free states these two residues fall apart (Figure 5A,B). When these two residues interact with ATP, they also bring together αD

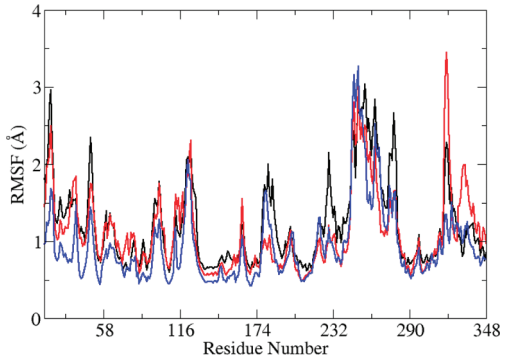

FIGURE 6: RMSF vs residue plot for p38γU (black), p38γP (red), and p38γP-ATP (blue).

and β7 and therefore modify the position of the αD-αE loop with respect to the β7-β8 loop, the two loops that form the DEJL docking site. In this sense, ATP performs direct interactions with residues that govern the dynamics and the conformation of the DEJL docking site important for protein−protein interactions. It is interesting to remark that along the simulations both conformations, with D115 and G157 near and far away, are visited, but the populations are changed. In the ATP-bound state these residues are most of the time near while in the ATP-free states they are mostly far away. Our result indicates that the change in conformation and more importantly in the dynamics that we observed in solution may not be observed in the crystal structures. In this sense, the changes observed in the different MAPKs crystals indicate relevant but small changes in the conformation of the DEJL docking site as we observe in the p38γ case. However, changes in the dynamics, as we will discuss in detail in the next sections, seem to be more important. As the networks of interactions seem to be conserved in the MAPK family, JNK1, ERK2, and p38α, all have a polar residue in the D115 position with a carboxyl moiety free to interact with the OH from the ribose (aspartic acid in ERK2 and p38α and asparagine in JNK1); we believe that similar changes may be observed in the dynamics of other MAPKs. We show in Supporting Information the case of the only other wild-type structure of a MAPK with ATP, the structure of JNK3 with ANP in the inactive state (PDB: 1JNK) (Supporting Information Figure S11). We see similar interactions of two residues located in the same moieties as in p38γ; D115 is replaced by an asparagine that has a hydrogen bond with the OH of the ribose and the carboxyl from the backbone of a serine is in a similar position as the carboxyl of G157 interacting with the other OH from ATP. Taking this into account, we expect that similar results should be observed for the other MAPKs. We have identified key interactions of the protein with the ATP moiety that may be regulating the dynamics of DEJL docking by an allosteric mechanism that seems to be conserved in other MAPKs. As we will show in the following sections, we can see changes in the global dynamics of the three states that corroborate what to expect by the changes in the interactions described above.

Another way to study the conformations visited during the MD is to analyze the projection histograms of the first EMs and scatter plots of EM1 vs EM1, shown in Supporting Information Figures S3 and S4. The results show that the first mode is bimodal for all states, which results in two different conformational substates. Moreover, for p38γU and p38γP-ATP also the second mode is bimodal, resulting in up to four different substates. Detailed analysis of the EM shows that conformational substates are mostly due to changes in the MAPK insert relative position. In all cases, the RMSD between the conformations of the substates is below 2.0 Å, meaning that changes between substates are small.

Changes in the Dynamics of p38γ in the Three States. To gain a first insight into p38γ dynamical fluctuations, we computed the RMSF vs residue plot for all three states, as shown in Figure 6. To check reproducibility of the results, we calculated the RMSF for the last 100 ns of the simulations and repeated the calculations for the last 50 ns; the obtained results were similar as we show in Supporting Information Figure S6. The fluctuation pattern is similar for all systems; the most flexible region corresponds to the MAPK insert (residues 245−290), presenting fluctuations of more than 3 Å. The second region showing high mobility in all systems corresponds to the C-terminal loop and L16 helix (residues 312 to Ct); interestingly, for this region mobility is highest in p38γP. Other common regions with high mobility are the hinge region, the αD-αE loop part of the DEJL docking site (residues 96−124), and the phosphorylation lip and P + 1 sites (residues 180−204).

Looking at the differences between the systems, the first big difference consists of the peaks observed in p38γU corresponding to G and H helices that flank the MAPK insert, whose mobility is reduced upon phosphorylation and ATP binding. This change may be regulating the changes observed in the intrinsic dynamics of the MAPK insert (see below). The second significant change is observed for the whole N-terminal domain, the hinge region, and ATP binding site (residues 1−175 and 312−350) whose whole mobility is significantly reduced upon ATP binding, which suggests that specific interactions of the ATP molecule tend to stabilize the N-terminal domain.

(*A*) *Essential Mode Analysis*. To further characterize each p38γ system dynamics and reveal the nature of the concerted motions of potential functionality, several EM analyses were performed as described in the Computational Methods section. Table S2 (Supporting Information) shows the EM contribution to the overall dynamics for each state and the structural regions involved in the first five EMs.

The data from Supporting Information Table S2 show that five motions account for about 70% of the structural dynamics; the first EM has a notably high contribution (almost 40%) especially in p38γU and p38γP, showing that concerted and possibly functional motions of the structural elements can be described with the first three to four modes. Visual inspection of the corresponding EM shows that for all cases EMs are distributed in more than one protein region, a fact that probably reflects the size and complexity of MAPK dynamics. Generally, and consistent with data shown above, the main segments showing concerted motions are the MAPK insert, the DEJL docking site, and the Nt domain.

For the p38γU state, the first and second EM show concerted motions of the Nt domain. MAPK insert motions appear in EM1, EM2, and EM3. EM1 shows also movements of αL14-αH and αI-αL16 loops and the D helix. The second EM also has a main contribution from a wide up/down motion of the P lip. Finally, EM4 is localized in the Ct loops and the Nt domain loops. For the p38γP state, the EM1 has a big contribution of the whole Nt domain, including the DEJL site, and also the MAPK insert. Interestingly, EM1 and EM2 both display different open/close movements of the DEJL docking site. EM2 also shows minor movement of the P lip. It is important to note that even though EM1 and EM2 from p38γU and p38γP are similarly

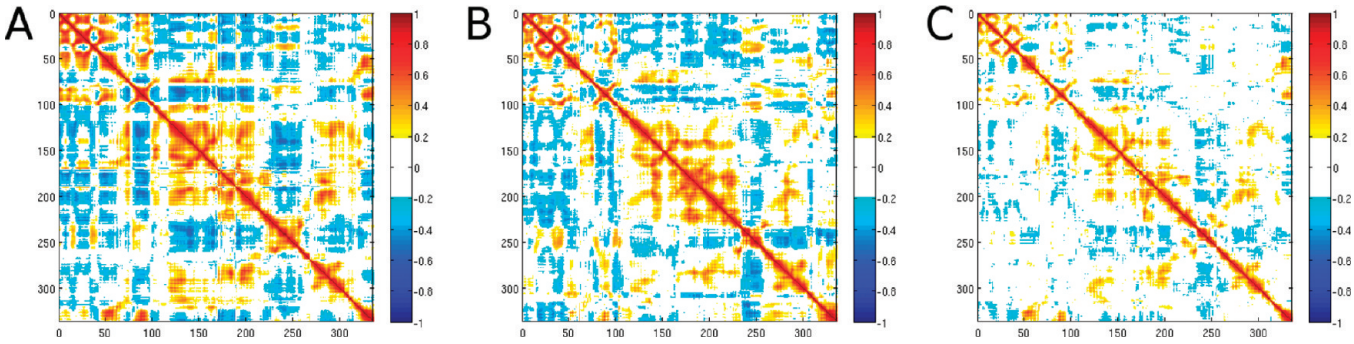

FIGURE 7: Cross-correlation motion plots: (A) p38γU; (B) p38γP; (C) p38γP-ATP.

localized, their movements are significantly different. p38γP EM3 shows mobility of the hinge region affecting the DEJL docking site and also the C-terminal loops. It is interesting to remark that the EMs of the two states that involve the transition from inactive to active are localized in regions that have been associated with protein−protein interactions and activity, suggesting a relation between dynamics and protein function. Our results indicate that upon dephosphorylation the essential dynamics of the protein is changed even though the involved regions are similar. In the case of the DEJL docking site and the MAPK insert, phosphorylation may be regulating p38γ protein associations and therefore specificity by generating changes in the dynamics of the docking sites, something that has been difficult to capture by previous experimental approaches. For the p38γP-ATP system, the first EM shows as the main contribution a big movement of the MAPK insert together with helices G and H and its connecting loops, the P + 1 site loop, and the DEJL site with an open/close movement. The second EM in this case is localized in the whole Nt domain which shows also contributions from the DEJL docking site and concerted motions of the phosphorylation lip. The MAPK insert motion is also present in EM3, EM4, and EM5.

In summary, p38γ dynamics shows that a common motion pattern is present in all three states with the MAPK insert as the dominant flexible element, which as discussed before distinguishes conformation subpopulations and the Nt domain and loops following. However, as described in detail, the magnitude and type of motion are characteristic of each state.

(*B*) *Cross-Correlation Motions*. Another informative way for analyzing the dynamics of a protein is to compute the residue to residue cross-correlation motion matrix (Figure 7), as defined in the Computational Methods section.

The results show notable differences between the three states. Activation of p38γ and ATP binding both tend to retain the global pattern but to localize the correlated motions to a few key residues, pointing toward a more ordered dynamics of specific structural elements of the protein. For all cases, related motions are located mainly in the Nt domain, including helix L16, and in the central region (αD and αE, β7 to β9, the phosphorylation lip, and P + 1 site) whose motions are correlated altogether and with helices H and I. Interestingly, also the loops forming the DEJL site are correlated in the three states. These results are in agreement with the EM analysis presented before where concerted complex motions of the proteins were observed in the case of p38γP and p38γP-ATP, meaning that in the phosphorylated and ATP-bound states the structure changes together with the dynamics to produce an *active* enzyme.

As mentioned above, we have computed the conformational entropy for the three states. The obtained values correspond to a 57 kcal/mol (T = 298 K) net change upon dephosphorylation and a 19 kcal/mol (T = 298 K) net change for the unbinding of ATP from the active state, meaning that dephosphorylation/phosphorylation produces a bigger reduction in entropy as compared to ATP unbinding/binding, in agreement with the EM calculations and the cross-correlation results shown above, supporting the idea that when the protein gets activated, the protein motions become more organized with concomitant entropy loss.

Having shown the conformational and dynamical changes in p38γ upon activation/deactivation and ATP unbinding/binding, we will now characterize the transition between each state's dynamical ensemble.

The Deactivation/Activation and ATP Unbinding/Binding Transitions in p38γ. To characterize the transition between the three states, we computed the combined EM of two dynamics: p38γU and p38γP to represent the activation/deactivation transition and p38γP with p38γP-ATP to represent the ATP unbinding/binding transition. In these cases the first EM (the transition mode) captures the conformational transition that best represents the change between both ensembles. Supporting Information Figure S12 shows the corresponding transition modes projected on the p38γ structure.

The first essential mode (Supporting Information Figure S12A) for the activation transition produces coordinated changes of different regions: the closing of the activation lip, movements of the whole Nt domain that closes the active site region, a rotation of the MAPK insert and helix G with respect to C-terminal domain, and a reorganization of the D-helix and the β7-β8 loop, the DEJL docking site. The changes in the MAPK insert correspond to a concerted movement of both MAPK helices together with helix G that move further apart from the αH-αI loop toward the end of αF (the distance between the αH-αI loop and the α1L14-α2L14 loop increases from 14.85 Å in p38γU to 18.28 Å in p38γP). The first essential mode for the change between the ATP-unbound and -bound states shows further movement of the MAPK insert and a small closing of the P lip. Changes are also observed in the Nt domain, now localized in helices C and L16, that further close the ATP pocket. Our results indicate that changes upon activation are spread in the MAPK fold and involve specific regions of the protein that are not directly connected to the activation lip such as the reorientation of the two domains (see detailed section below), closing of the P lip, and reorganization of the dynamics of the docking sites. Reorientation between the domains and changes in helix C have also been proposed by recent studies of relevant conformational changes of other kinases (*23*, *24*).

Projection of the transition modes along the dynamics of each state and conformation population analysis allows a comparison

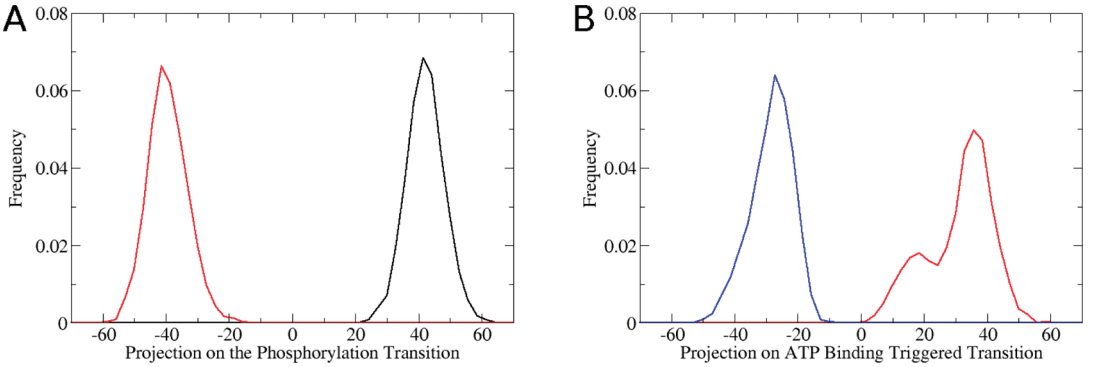

FIGURE 8: Histograms of each MD simulation snapshot on the conformational transition EM. (A) p38γU (black) and p38γP (red) dynamics projected on the phosphorylation transition. (B) p38γP (red) and p38γP-ATP (blue) dynamics projected on ATP binding triggered transition.

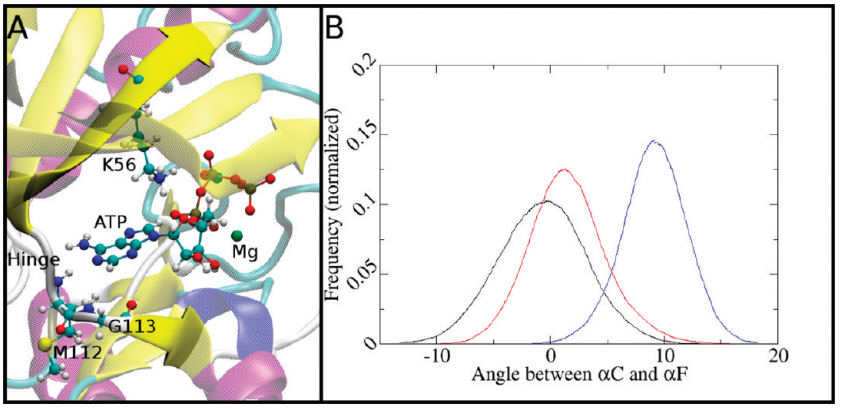

FIGURE 9: (A) Interaction between H of Met-112 and N1 of the ATP molecule. (B) Histograms of the αC and αF angle vs time plot: black for p38γU, red for p38γP, and blue for p38γP-ATP.

of the magnitude of the equilibrium fluctuations in one state, with that corresponding to the conformational transition between states. Histograms of the projected dynamics along both transition modes are shown in Figure 8. An expected result is that the dephosphorylation/phosphorylation of p38γ produces a much bigger transition compared to that of ATP unbinding/binding. Activation triggers an average 0.24 Å shift per backbone atom, compared to an about 0.13 Å shift per backbone atom due to ATP binding. The equilibrium dynamics of p38γU and p38γP are completely separated in activation transition space, while p38γP and p38γP-ATP equilibrium dynamics almost overlap each other. It is interesting to remark that both starting states, p38γU and p38γP, show wider conformational amplitude projected on their transitions compared to the end states, which show exploration of a narrower conformational space.

Finally, to relate equilibrium dynamics with the transition between the different states, we computed the involvement coefficients (IC) of each equilibrium EM to the p38γU to p38γP and p38γP to p38γP-ATP transition, determined by the transition mode; the results are shown in Table S3 (Supporting Information).

The results from Supporting Information Table S3 clearly show that equilibrium motions of MAPK are related with the activation and ATP binding mechanism. The first and second EM of p38γU for example are significantly related with the phosphorylation transition, with a less but important relation of EM4 and EM5. Interestingly, for p38γP EM1 is completely unrelated to activation (back-transition) but significantly related with ATP-induced change. However, in p38γP-ATP EM1 is related to the ATP binding transition, possibly related to the ADP release mechanism. These data clearly show that the fluctuations of the equilibrium states of p38γ are similar to the conformational transitions observed upon activation and ATP binding.

Two main changes have been observed in the dynamics of the three states, the reorientation between the domains and the plasticity of the DEJL docking site and the MAPK insert. These changes are now discussed in detail.

(*A*) *Domain−Domain Orientation*. Most of the observed changes in the N-terminal domain reflect global domain rotation movements with respect to the C-terminus, something that has been proposed in previous studies on ERK2 and p38α (*9*, *19*−*21*, *41*). To characterize this domain rotation, we measured the angle formed by helices αC and αF along the dynamics for the three states (Figure 9); we subtracted the angle of p38γU to all results for clarity's sake. We show the time evolution of the angle in Supporting Information Figure S7; as can be seen, good sampling is achieved as expected for a well-converged simulation. As shown in Figure 9, in the phosphorylated state, the equilibrium position of the angle is slightly shifted, but also the amplitude of the movement is significantly reduced. In the ATP-bound state, a bigger rotation is observed, and the mobility is further reduced in agreement with previous results (*19*, *20*). To further understand the changes between the states, we analyzed a key element regulating MAPK dynamics, the hinge region (Table 1) (*42*). We measured the ϕ/ψ angles of the hinge residues, 110−114, along the simulation and found important changes only for M112 and G113. The ϕ/ψ position of the G113 residue in

p38γP is in between the α and β regions (−70, −30) during the whole simulation. However, when ATP is in the active site, a new conformation is observed, with ϕ/ψ values of (−150, 150) that can be explained because the adenine moiety of ATP is able to interact with the backbone of G113 (Figure 9) leading to a stabilization of the new conformer. Probably, this interaction reduces also the mobility of the N-terminal domain. The change of the NH position in G113 leads also to a rotation of the backbone CO of M112; ψ changes from the β region to the α region in the Ramachandran plot. It is interesting to remark that neither the carbonyl of P110 nor the NH of M112, that are interacting with ATP by hydrogen bonds, changes its conformation in the three states, indicating that these residues are already in position for the binding of ATP. Another interaction that also contributes to this change is the formation of a stable salt bridge between K56 and the β-phosphate group of ATP. As K56 belongs to β3, the interaction with ATP closes the pocket, inducing the rotation of the N-terminus and also lowering the flexibility of this moiety. The important point is that ATP has specific interactions with key residues in p38γ and therefore is the one triggering the biggest change in the domain−domain orientation.

(*B*) *Structural and Dynamical Effects upon Dephosphorylation/Phosphorylation and ATP Unbinding/Binding on the Docking Sites*. As mentioned in the introduction, two docking sites (DS) have been described for MAPK. The first site, named the DEJL site, has been identified in different MAPKs and binds linear peptides between the αD-αE and β7-β8 loops together with an acidic patch. The second site, called FXFP, has been identified in ERK2 and p38α and lies between the MAPK insert, helix αG, and the P + 1 site. As we pointed out before, the DEJL docking site participates in the essential modes of the protein upon phosphorylation and ATP binding. The coordinated movements involved the opening and closing of the region that binds the $Ø_A$-X-$Ø_B$ motif of other proteins. The transition from inactive to active involves the movement of the β7-β8 loop toward the N-terminal domain as the whole domain reorientates, finally accommodating the ATP. When we inspect the interactions governing the dynamics of the β7-β8 loop, we found that T114 from the hinge region is interacting by a double hydrogen bond with V161 from β7. Interestingly, we found that these interactions are coordinated with movements of the loop; in p38γU the T114 CO−V161 NH hydrogen bond is broken, in p38γP only the T114 NH−V161 CO hydrogen bond is broken, and in p38γP-ATP both hydrogen bonds are formed. This small change in the hydrogen bond network helps to regulate the loop dynamics together with the hinge region and the interactions observed by the ribose of ATP. In this sense, activation/deactivation and ATP unbinding/binding shifted the equilibrium of key interactions that promote bigger changes in the overall structural organization.

Even though the FXFP site has not been described in p38γ, by comparison, the residues defining the site are L191 and I197 from the P + 1 site, L232, L235, and M239 from αG, and A258, Y261, and L265 from the MAPK insert. As we described above, key interactions of these residues are changed in the active state as the whole MAPK insert moves, changing the accessibility of this region. In agreement with the change in interactions we see a change in the dynamics. We found that the MAPK insert is a highly flexible moiety as judged by the RMSF calculation and that it contributes importantly to the first five EMs. By inspecting the EMs and the cross-correlation motions, we found that the MAPK insert becomes more dynamically structured as the protein becomes phosphorylated and binds ATP. The dynamics of the two helices of the MAPK insert goes from disorganized to organized motions upon activation. In the p38γP-ATP state the two helices move together, opening and closing the region corresponding to protein binding. We believe that even though this docking site has not been determined for p38γ, the correlated motions should be conserved upon different members of the MAPK family. Besides helix G, two small loops seem to regulate MAPK insert dynamics according to our simulations, one formed by residues 243−246 and the other one by residues 265−272. There are three hydrogen bonds between these two loops; the OH of T244 is interacting with the NH and CO of L265 and the NH of T244 is interacting with the CO of L265. We found that these interactions are weakened in p38γU in comparison to the p38γP and p38γP-ATP states, meaning that the equilibrium is shifted to conformations where the hydrogen bonds are not formed. These changes produce a disorganization of the movements of the two helices that form the MAPK insert. As we pointed out before, changes in the activation loop lead to changes in zones that are far away, regulating the dynamics of specific motifs.

DISCUSSION

Even though the MAPK structure has been extensively studied, we still do not have a clear picture of how its function is regulated at the molecular level (*4*). Several studies pointed out that protein dynamics and allostery play an important role in the regulation of MAPK function (*9*, *19*−*21*, *42*, *6*, *8*); however, studying protein dynamics and allosterism from a structural view is difficult. While traditional structure atomic resolution techniques such as X-ray crystallography yield only a static picture of MAPK in different states, those techniques that can measure protein dynamics such as spectroscopic and fluorescence-based methods are unable to provide atomistic detail. Hydrogen exchange and EPR techniques are very powerful and allow a better insight; however, the interpretation and analysis are still indirect and do not have atomic resolution. Long molecular dynamics simulations offer the possibility to fill this gap, allowing the analysis of protein motions, allosteric transitions, and its relation to function with atomistic detail (*43*). Therefore, to complement previous experimental results in this work, we have used molecular dynamics techniques to study the dynamical changes associated with p38γ activation/deactivation and ATP binding/unbinding.

Relation with Hydrogen Exchange Experiments. Principal experimental evidence on the change in MAPK dynamics upon activation and ATP binding comes from hydrogen exchange (HX) studies performed on ERK and p38α (*9*, *21*, *42*). Data for both proteins show high HX patterns mainly in MAPK insert, P lip, and several loops, while low exchange is observed for helices C, E, and F and sheets 3 and 4, results that reflect differential solvent accessibility of these zones. HX data also revealed interesting changes in mobility or solvent accessibility in ERK2 and p38α that could not be explained by the available X-ray data. In both proteins a reduction of the HX rates for the F and G helices was observed (*9*, *17*, *19*, *20*). Our data show that phosphorylation significantly reduces G and H helix mobility and to some extent helix F and that significant changes are also observed in the MAPK insert dynamics, in agreement with the HX data. For p38α several Nt regions also showed a decrease in their HX pattern, a fact attributed to reduced mobility of these regions. In the same line of evidence, our results show that

significant reduction and ordering of the Nt domain mobility occur upon activation and ATP binding. HX rates were also reduced in the β7-β8 loop for p38α and the Gly-rich loop in ERK2 upon activation. In p38γ both zones reduce their mobility upon phosphorylation, explaining the observed trend. In summary, the dynamical information obtained here for p38γ is in good agreement with data obtained for p38α and ERK2, pointing to a common MAPK activation induced change in protein dynamics.

The Open/Close Model for MAPK Function. Based on HX rate changes observed due to ATP binding in native and phosphorylated ERK2, the authors proposed a two-state open/close model for ERK function (*9*, *17*, *19*, *20*). In the corresponding model ATP would bind to the Nt domain in the open state, leaving the DFG loop (residues 171−173 in p38γ) exposed. The closed structure would partially bury the DFG loop, reducing the observed HX rates. Phosphorylation would favor the closed state, explaining the observed differences. The MD simulations reveal the presence of a conformational transition (shown in Figure 9) that represents the closing of the Nt domain in the phosphorylated and ATP-bound states. However, our simulations do not clearly separate the system in two conformations, open and close, but suggest a shift in the equilibrium from the inactive to the phosphorylated ATP-bound state. We cannot rule out that an even more opened conformation exists which is favored in the inactive state. Another possibility is that conformational changes in ERK2 are of a greater magnitude when compared to p38γ studied here.

Which Model, Population Shift or Induced Fit, Better Describes p38γ Conformational Changes? Understanding how local modifications are propagated to the rest of the protein leading to significant transitions in its structure and activity (or allostery) is a key element in the knowledge of how proteins work. The theoretical framework for thinking allosterism includes both thermodynamic and stereochemical formulations. Mechanistically, in the stereochemical view, the activation event causes a local conformational change that is propagated through residue to residue contacts to the rest of the protein. The propagation occurs through well-defined structural pathways and involves specific amino acids. The other scheme, also known as the population shift model, implies that the "activated conformation" is already present with nonnegligible population in the nonactivated conformational ensemble, and therefore the activation merely shifts the equilibrium. The most relevant implication of the population shift model is that, in order to populate the active state, protein equilibrium dynamics must include motions related to the allosteric transition (*44*).

The fact that phosphorylation of Tyr/Thr produces several new charge−charge interactions with several arginines, that are impossible to be formed by the nonphosphorylated residues, together with the data from Figure 8 showing the big distance between the p38γU and p38γP dynamics along the transition, suggests that the stereochemical model may be suitable for describing the p38γ activation transition. Furthermore, the EM and fluctuation analysis show that protein dynamics is also significantly different between both states, further supporting the existence of two clearly different states with unrelated energy surfaces. Despite the fact that we have shown evidence that relatively good convergence has been achieved, due to the length of the simulations we cannot ruled out that at longer time periods the conformations associated with the closing of the activation loop could be observed. Binding of ATP, on the other hand, produces a smaller change, as judged by the results presented in previous sections. The smaller change, together with the data showing (i) that equilibrium conformations almost overlap along the structural transisition (Figure 8 transition histograms), (ii) the analysis of the hinge residue ϕ/ψ values showing the presence of two similar states for p38γP and p38γP-ATP systems with a clear change in the state's populations due to ATP binding, and (iii) the high values for the IC of the equilibrium EM (especially the first in both cases) to the transition mode, all make a strong point for a population shift transition due to ATP binding. These results have important implications in active research areas, the design of MAPK inhibitors (*45*−*47*) and intrinsically active MAPKs (*48*−*51*).

CONCLUSIONS

Our results show that phosphorylation/dephosphorylation and ATP binding/unbinding trigger allosteric changes that modify p38γ structure but more significantly its dynamics, resulting in more ordered motions in the active/ATP-bound protein. Interestingly, the allosteric changes are located in the previously described docking sites important for protein−protein interactions and therefore for MAPK module assemblage and cascade specificity. Our data also show that activation transition is more likely to be represented by the stereochemical model of allostery, while the change due to ATP binding possibly represents a population shift toward catalytic prone conformations. In summary, our results complement previous experimental studies giving a broader picture of MAPK structure/dynamics to function relationships, which may have a profound impact for the design and understanding of intrinsically active MAPK and inhibitors.

SUPPORTING INFORMATION AVAILABLE

Figures corresponding to the first two EM in the structure of p38γ; the EM projection on the dynamics for the first three modes for each state; the EM histograms for the first three EMs in each state; the scatter plots for EM1 vs EM2 for the three states; the entropy calculation for the three states; the RMSF for the last 50 ns for the three states; the time evolution of the angle between helices αC and αF for the three states; the contact maps for each state of p38γ; and figures comparing the previous crystallized structures of other MAPKs. This material is available free of charge via the Internet at http://pubs.acs.org.

REFERENCES

1. Kyriakis, J. M., and Avruch, J. (2001) Mammalian mitogen-activated protein kinase signal transduction pathways activated by stress and inflammation. *Physiol. Rev. 81*, 807–869.
2. Widmann, C., Gibson, S., Jarpe, M. B., and Johnson, G. L. (1999) Mitogen-activated protein kinase: conservation of a three-kinase module from yeast to human. *Physiol. Rev. 79*, 143–180.
3. Bellon, S., Fitzgibbon, M. J., Fox, T., Hsiao, H. M., and Wilson, K. P. (1999) The structure of phosphorylated p38gamma is monomeric and reveals a conserved activation-loop conformation. *Structure 7*, 1057–1065.
4. Goldsmith, E. J., Cobb, M. H., and Chang, C. I. (2004) Structure of MAPKs. *Methods Mol. Biol. 250*, 127–144.
5. Liu, S., Sun, J. P., Zhou, B., and Zhang, Z. Y. (2006) Structural basis of docking interactions between ERK2 and MAP kinase phosphatase 3. *Proc. Natl. Acad. Sci. U.S.A 103*, 5326–5331.
6. Shaw, D., Wang, S. M., Villasenor, A. G., Tsing, S., Walter, D., Browner, M. F., Barnett, J., and Kuglstatter, A. (2008) The crystal structure of JNK2 reveals conformational flexibility in the MAP kinase insert and indicates its involvement in the regulation of catalytic activity. *J. Mol. Biol. 383*, 885–893.
7. White, A., Pargellis, C. A., Studts, J. M., Werneburg, B. G., and Farmer, B. T., II (2007) Molecular basis of MAPK-activated protein kinase 2:p38 assembly. *Proc. Natl. Acad. Sci. U.S.A. 104*, 6353–6358.

8. Zhou, T., Sun, L., Humphreys, J., and Goldsmith, E. J. (2006) Docking interactions induce exposure of activation loop in the MAP kinase ERK2. *Structure 14*, 1011–1019.
9. Hoofnagle, A. N., Stoner, J. W., Lee, T., Eaton, S. S., and Ahn, N. G. (2004) Phosphorylation-dependent changes in structure and dynamics in ERK2 detected by SDSL and EPR. *Biophys. J. 86*, 395–403.
10. Zarubin, T., and Han, J. (2005) Activation and signaling of the p38 MAP kinase pathway. *Cell Res. 15*, 11–18.
11. Turjanski, A. G., Vaque, J. P., and Gutkind, J. S. (2007) MAP kinases and the control of nuclear events. *Oncogene 26*, 3240–3253.
12. Tanoue, T., and Nishida, E. (2003) Molecular recognitions in the MAP kinase cascades. *Cell. Signalling 15*, 455–462.
13. Remenyi, A., Good, M. C., and Lim, W. A. (2006) Docking interactions in protein kinase and phosphatase networks. *Current Opin. Struct. Biol. 16*, 676–685.
14. Greenman, C., Stephens, P., Smith, R., Dalgliesh, G. L., Hunter, C., Bignell, G., Davies, H., Teague, J., Butler, A., Stevens, C., Edkins, S., O'Meara, S., Vastrik, I., Schmidt, E. E., Avis, T., Barthorpe, S., Bhamra, G., Buck, G., Choudhury, B., Clements, J., Cole, J., Dicks, E., Forbes, S., Gray, K., Halliday, K., Harrison, R., Hills, K., Hinton, J., Jenkinson, A., Jones, D., Menzies, A., Mironenko, T., Perry, J., Raine, K., Richardson, D., Shepherd, R., Small, A., Tofts, C., Varian, J., Webb, T., West, S., Widaa, S., Yates, A., Cahill, D. P., Louis, D. N., Goldstraw, P., Nicholson, A. G., Brasseur, F., Looijenga, L., Weber, B. L., Chiew, Y. E., Defazio, A., Greaves, M. F., Green, A. R., Campbell, P., Birney, E., Easton, D. F., Chenevix-Trench, G., Tan, M. H., Khoo, S. K., Teh, B. T., Yuen, S. T., Leung, S. Y., Wooster, R., Futreal, P. A., and Stratton, M. R. (2007) Patterns of somatic mutation in human cancer genomes. *Nature 446*, 153–158.
15. Chang, C. I., Xu, B. E., Akella, R., Cobb, M. H., and Goldsmith, E. J. (2002) Crystal structures of MAP kinase p38 complexed to the docking sites on its nuclear substrate MEF2A and activator MKK3b. *Mol. Cell 9*, 1241–1249.
16. Heo, Y. S., Kim, S. K., Seo, C. I., Kim, Y. K., Sung, B. J., Lee, H. S., Lee, J. I., Park, S. Y., Kim, J. H., Hwang, K. Y., Hyun, Y. L., Jeon, Y. H., Ro, S., Cho, J. M., Lee, T. G., and Yang, C. H. (2004) Structural basis for the selective inhibition of JNK1 by the scaffolding protein JIP1 and SP600125. *EMBO J. 23*, 2185–2195.
17. Lee, T., Hoofnagle, A. N., Kabuyama, Y., Stroud, J., Min, X., Goldsmith, E. J., Chen, L., Resing, K. A., and Ahn, N. G. (2004) Docking motif interactions in MAP kinases revealed by hydrogen exchange mass spectrometry. *Mol. Cell 14*, 43–55.
18. Zhang, J., Zhou, B., Zheng, C. F., and Zhang, Z. Y. (2003) A bipartite mechanism for ERK2 recognition by its cognate regulators and substrates. *J. Biol. Chem. 278*, 29901–29912.
19. Hoofnagle, A. N., Resing, K. A., Goldsmith, E. J., and Ahn, N. G. (2001) Changes in protein conformational mobility upon activation of extracellular regulated protein kinase-2 as detected by hydrogen exchange. *Proc. Natl. Acad. Sci. U.S.A 98*, 956–961.
20. Lee, T., Hoofnagle, A. N., Resing, K. A., and Ahn, N. G. (2005) Hydrogen exchange solvent protection by an ATP analogue reveals conformational changes in ERK2 upon activation. *J. Mol. Biol. 353*, 600–612
21. Sours, K. M., Kwok, S. C., Rachidi, T., Lee, T., Ring, A., Hoofnagle, A. N., Resing, K. A., and Ahn, N. G. (2008) Hydrogen-exchange mass spectrometry reveals activation-induced changes in the conformational mobility of p38alpha MAP kinase. *J. Mol. Biol. 379*, 1075–1093.
22. Dwivedi, P. P., Hii, C. S., Ferrante, A., Tan, J., Der, C. J., Omdahl, J. L., Morris, H. A., and May, B. K. (2002) Role of MAP kinases in the 1,25-dihydroxyvitamin D3-induced transactivation of the rat cytochrome P450C24 (CYP24) promoter. Specific functions for ERK1/ERK2 and ERK5. *J. Biol. Chem. 277*, 29643–29653.
23. Berteotti, A., Cavalli, A., Branduardi, D., Gervasio, F. L., Recanatini, M., and Parrinello, M. (2009) Protein conformational transitions: the closure mechanism of a kinase explored by atomistic simulations. *J. Am. Chem. Soc. 131*, 244–250.
24. Yang, S., Banavali, N. K., and Roux, B. (2009) Mapping the conformational transition in Src activation by cumulating the information from multiple molecular dynamics trajectories. *Proc. Natl. Acad. Sci. U.S.A. 106*, 3776–3781.
25. Patel, S. B., Cameron, P. M., Frantz-Wattley, B., O'Neill, E., Becker, J. W., and Scapin, G. (2004) Lattice stabilization and enhanced diffraction in human p38 alpha crystals by protein engineering. *Biochim. Biophys. Acta 1696*, 67–73.
26. Hornak, V., Abel, R., Okur, A., Strockbine, B., Roitberg, A., and Simmerling, C. (2006) Comparison of multiple Amber force fields and development of improved protein backbone parameters. *Proteins 65*, 712–725.
27. Case, A., Pearlman, D. A., Caldwell, J. W., Cheatham, T. E., Wang, J. M., Ross, W. S., Simmerling, C., Darden, T., Merz, K. M., Stanton, R. V., Cheng, A., Vincent, J. J., Crowley, M., Tsui, V., Gohlke, H., Radmer, R., Duan, Y., Pitera, J., Massova, I., Seibel, G. L., Singh, U. C., and Weiner, P. A. (2002) Amber 7, University of California, San Francisco.
28. Craft, J. W., Jr., and Legge, G. B. (2005) An AMBER/DYANA/MOLMOL phosphorylated amino acid library set and incorporation into NMR structure calculations. *J. Biomol. NMR 33*, 15–24.
29. Meagher, K. L., Redman, L. T., and Carlson, H. A. (2003) Development of polyphosphate parameters for use with the AMBER force field. *J. Comput. Chem. 24*, 1016–1025.
30. Jorgensen, W. L., Chandrasekhar, J., Madura, J. D., Impey, R. W., and Klein, M. L. (1983) Comparison of simple potential functions for simulating liquid water. *J. Chem. Phys. 79*, 926–935.
31. Turjanski, A. G., Hummer, G., and Gutkind, J. S. (2009) How mitogen-activated protein kinases recognize and phosphorylate their targets: a QM/MM study. *J. Am. Chem. Soc. 131*, 6141–6148.
32. Turjanski, A. G., Estrin, D. A., Rosenstein, R. E., McCormick, J. E., Martin, S. R., Pastore, A., Biekofsky, R. R., and Martorana, V. (2004) NMR and molecular dynamics studies of the interaction of melatonin with calmodulin. *Protein Sci. 13*, 2925–2938.
33. Berendsen, H. J. C., Postma, J. P. M., Vangunsteren, W. F., Dinola, A., and Haak, J. R. (1984) Molecular dynamics with coupling to an external bath. *J. Chem. Phys. 81*, 3684–3690.
34. Essmann, U., Perera, L., Berkowitz, M. L., Darden, T., Lee, H., and Pedersen, L. G. (1995) A smooth particle mesh Ewald method. *J. Chem. Phys. 103*, 8577–8593.
35. Hayward, S., and de Groot, B. L. (2008) Normal modes and essential dynamics. *Methods Mol. Biol. 443*, 89–106.
36. Capece, L., Estrin, D. A., and Marti, M. A. (2008) Dynamical characterization of the heme NO oxygen binding (HNOX) domain. Insight into soluble guanylate cyclase allosteric transition. *Biochemistry 47*, 9416–9427.
37. Nadra, A. D., Marti, M. A., Pesce, A., Bolognesi, M., and Estrin, D. A. (2008) Exploring the molecular basis of heme coordination in human neuroglobin. *Proteins 71*, 695–705.
38. Schlitter, J. (1993) Estimation of absolute and relative entropies of macromolecules using the covariance matrix. *Chem. Phys. Lett. 215*, 617–621.
39. Heemskerk, F. M., Zorad, S., Xu, N., Gutkind, S. J., and Saavedra, J. M. (1999) Characterization of AT2 receptor expression in NIH 3T3 fibroblasts. *Cell. Mol. Neurobiol. 19*, 277–288.
40. Humphrey, W., Dalke, A., and Schulten, K. (1996) VMD: visual molecular dynamics. *J. Mol. Graphics 14*, 33–38.
41. Canagarajah, B. J., Khokhlatchev, A., Cobb, M. H., and Goldsmith, E. J. (1997) Activation mechanism of the MAP kinase ERK2 by dual phosphorylation. *Cell 90*, 859–869.
42. Emrick, M. A., Lee, T., Starkey, P. J., Mumby, M. C., Resing, K. A., and Ahn, N. G. (2006) The gatekeeper residue controls autoactivation of ERK2 via a pathway of intramolecular connectivity. *Proc. Natl. Acad. Sci. U.S.A. 103*, 18101–18106.
43. Zhang, J., Li, C., Chen, K., Zhu, W., Shen, X., and Jiang, H. (2006) Conformational transition pathway in the allosteric process of human glucokinase. *Proc. Natl. Acad. Sci. U.S.A. 103*, 13368–13373.
44. Boehr, D. D., Nussinov, R., and Wright, P. E. (2009) The role of dynamic conformational ensembles in biomolecular recognition. *Nat. Chem. Biol. 5*, 789–796.
45. Bogoyevitch, M. A., Ngoei, K. R., Zhao, T. T., Yeap, Y. Y., and Ng, D. C. (2010) c-Jun N-terminal kinase (JNK) signaling: recent advances and challenges. *Biochim. Biophys. Acta 1804*, 463–475.
46. Wong, K. K. (2009) Recent developments in anti-cancer agents targeting the Ras/Raf/ MEK/ERK pathway. *Recent Pat. Anticancer Drug Discov. 4*, 28–35.
47. Zhang, J., Shen, B., and Lin, A. (2007) Novel strategies for inhibition of the p38 MAPK pathway. *Trends Pharmacol. Sci. 28*, 286–295.
48. Yaakov, G., Bell, M., Hohmann, S., and Engelberg, D. (2003) Combination of two activating mutations in one HOG1 gene forms hyperactive enzymes that induce growth arrest. *Mol. Cell. Biol. 23*, 4826–4840.
49. Engelberg, D., and Livnah, O. (2006) Isolation of intrinsically active mutants of MAP kinases via genetic screens in yeast. *Methods* (*San Diego*) *40*, 255–261.
50. Levin-Salomon, V., Kogan, K., Ahn, N. G., Livnah, O., and Engelberg, D. (2008) Isolation of intrinsically active (MEK-independent) variants of the ERK family of mitogen-activated protein (MAP) kinases. *J. Biol. Chem. 283*, 34500–34510.
51. Askari, N., Beenstock, J., Livnah, O., and Engelberg, D. (2009) p38alpha is active in vitro and in vivo when monophosphorylated at threonine 180. *Biochemistry 48*, 2497–2504.